Paraventricular hypothalamic nucleus are essential for arousal promotion and maintenance

Zhi-Li Huang (huangzl@fudan.edu.cn)
Department of Pharmacology, School of Basic Medical Sciences; State Key Laboratory of Medical Neurobiology and MOE Frontiers Center for Brain Science, Fudan University, Shanghai
https://orcid.org/0000-0001-9359-1150

Chang-Rui Chen
Department of Pharmacology, School of Basic Medical Sciences; State Key Laboratory of Medical Neurobiology and MOE Frontiers Center for Brain Science, Fudan University, Shanghai

Yu-Heng Zhong
Department of Pharmacology, School of Basic Medical Sciences; State Key Laboratory of Medical Neurobiology and MOE Frontiers Center for Brain Science, Fudan University, Shanghai

Shan Jiang
Department of Pharmacology, School of Basic Medical Sciences; State Key Laboratory of Medical Neurobiology and MOE Frontiers Center for Brain Science, Fudan University, Shanghai

Wei Xu
Department of Pharmacology, School of Basic Medical Sciences; State Key Laboratory of Medical Neurobiology and MOE Frontiers Center for Brain Science, Fudan University, Shanghai

Zan Wang
Department of Neurology, The First hospital of Jilin University, Changchun

Lei Xiao
Fudan University

Wei-Min Qu
School of Basic Medical Sciences, State Key Laboratory of Medical Neurobiology and MOE Frontiers Center for Brain Science, Institutes of Brain Science, Fudan University https://orcid.org/0000-0002-0251-5214

Article

Keywords: circadian rhythm, wakefulness, sleep

Posted Date: January 27th, 2021

DOI: https://doi.org/10.21203/rs.3.rs-140209/v1

Abstract

Adequate wakefulness is fundamental for proper daytime functioning. Clinical observations indicate that the paramedian region of the hypothalamus is a critical node for controlling wakefulness. However, the specific nucleus and neural circuitry for this function remain unknown. Here, we found that inhibition of PVH^{vglut2} neurons induced 3-h increase of NREM sleep. Chemogenetic activation of PVH^{vglut2} neurons potently induced 9-h wakefulness, and PVH^{CRH} neuronal activation also exerted wakefulness. Photostimulation of PVH^{vglut2}→parabrachial complex/ventral lateral septum circuits immediately drove transitions from NREM to wakefulness. Furthermore, using in vivo fiber photometry or multichannel electrophysiological recordings in mice, we find arousal-dependent increases in population activity of PVH^{vglut2} neurons. Most importantly, ablation of PVH^{vglut2} neurons dramatically led mice to hypersomnia-like behaviors. These results demonstrate that PVH^{vglut2} neurons are essential for physiologic arousal in the hypothalamus.

Introduction

Hypersomnia is characterized by an irresistible need for sleep and an inability to stay awake during major waking episodes, which results in reduced function and overall worse quality of life and even induces mental diseases, highlighting its public health importance[1]. However, few dysfunctional wake-promoting nuclei have been identified to induce hypersomnia. Therefore, further identification of key nuclei and neural circuitry for promoting wakefulness represents a common goal for clinicians and researchers.

In the last 100 years, more than 15 wake-promoting nuclei have been identified. Von Economo first proposed a wake-active and promoting region located in the posterior hypothalamus from observations of marked somnolence in patients with epidemic encephalitis lethargic [2]. Furthermore, Moruzzi et al. and other studies have revealed that a brainstem ascending reticular activating system (ARAS) is responsible for wakefulness [3–5]. However, cell-body-specific ablation or inhibition of components of the ARAS—including the laterodorsal tegmentum (LDT), basal forebrain (BF), pedunculopontine tegmental nucleus (PPT) cholinergic neurons, dorsal raphe nucleus (DRN) serotonergic neurons, and locus coeruleus (LC) noradrenergic neurons—yields limited alterations in sleep [6–8]. Additionally, the lateral hypothalamic area (LH), parabrachial complex (PB), tuberomammilary nucleus (TMN), paraventricular nucleus of the thalamus (PVT), ventral tegmental area (VTA), and supramammillary nucleus (SUM) have also been demonstrated to be involved in arousal regulation [6,9–13]. However, among these wake-promoting nuclei, only LH orexinergic and PB glutamatergic neurons have been shown to be related to hypersomnia. Dysfunction of orexinergic neurons in the LH results in narcolepsy and sleep fragmentation [6,12,14,15]; PB glutamatergic neurons are considered to serve as a hub, as they receive afferent chemosensory information and play a role in triggering hypercapnia-induced arousal in obstructive sleep apnea (OSA), whereas ablation of PB glutamatergic neurons decreases hypercapnia-induced arousal [16–18]. The further amazing research found that ablation of LH orexinergic neurons and lateral parabrachial nucleus (L-PBN) glutamatergic neurons has little effect on sleep under baseline conditions, and deletion of vesicular

glutamate transporter 2 (vglut2) from the medial PB (MPB) causes only a modest (approximately 20%) reduction in wakefulness [8,14]. Clinically, patients with Parkinson's disease (PD), Alzheimer's disease (AD), Kleine-Levin Syndrome, and idiopathic hypersomnia (IH), in which LH orexinergic and PB glutamatergic neurons are thought to function normally, still show hypersomnolence [19]. Collectively, these results suggest that the key hypersomnolence control nucleus remains unidentified.

More than 90% of the PVH consists of glutamatergic neurons, whereas GABAergic neurons are more scarcely represented [20–22]. PVH^{vglut2} neurons co-express corticotropin-releasing hormone (PVH^{CRH}) [23], arginine vasopressin (PVH^{AVP}) [24,25]. In the present study, we used cutting-edge techniques in transgenic mice to elucidate that activation of PVH^{vglut2}, PVH^{CRH} neurons induced wakefulness. Conversely, ablation or suppression of PVH^{vglut2} neurons caused hypersomnia-like behaviors. Taken together, our findings indicate that the PVH is essential for wakefulness.

Results

PVH receives direct inputs from the PVT and PB. Considering that the homologous area of the primate posterior hypothalamus in rodents is around the PVH area, which contains mainly glutamatergic neurons, we examined the role of PVH^{vglut2} neurons in the regulation of wakefulness. We used Cre-dependent rabies virus–mediated monosynaptic retrograde tracing in Vglut2-Cre mice (Fig. 1a, b) and found that PVH^{vglut2} neurons received direct inputs from the PVT, PB, ZI and VLPAG (Fig. 1c-f), which are involved in sleep-wake control [9, 15–17,25,26], suggestion that the PVH might act as a key central node for sleep-wake regulation.

PVH^{vglut2} neurons are preferentially active during wakefulness. We next performed *in-vivo* fiber photometry to investigate the real-time activity of PVH^{vglut2} neurons across spontaneous sleep–wake cycles in freely moving mice. The recording mode for fiber photometery and the expression of the Cre-dependent AAVs expressing the fluorescent calcium indicator, GCaMP6f (AAV-EF1α-DIO-GCaMP6f), in the PVH of Vglut2-Cre mice are shown in Fig. 2a, b. PVH^{vglut2} neuronal activities during wakefulness were significantly higher than those during NREM sleep (Fig. 2c–e).

We next performed *in-vivo* multichannel electrophysiological recordings to monitor the spike firing of individual PVH neurons in freely behaving mice (Fig. 2f). PVH^{vglut2} neurons exhibited a higher firing rate during wakefulness than during sleep (Fig. 2g, h). The PVH^{vglut2} neuronal firing rate gradually decreased before sleep onset and increased during transitions from sleep to wakefulness (Fig. 2i–k). At the onset of behavioral arousal from NREM sleep, the mean firing rate reached 13.5 Hz (Fig. 2i). Collectively, these electrophysiological results clearly indicate a mechanistic framework for the activity-dependent participation of PVH neurons in the regulation of sleep and wakefulness.

Chemogenetic activation of PVH^{vglut2} and PVH^{CRH} neurons significantly increases wakefulness. Next, we investigated the activation effect of PVH^{vglut2} neurons in freely moving mice on wakefulness regulation

by injecting adeno-associated virus (AAV)-EF1α-double-floxed inverse-orientation (DIO)-hM3D(Gq)-mCherry into the PVH, respectively (Fig. 3a). At the beginning of the light phase (zeitgeber time 3 [ZT3]; 9:00), chemogenetic activation of PVH^{vglut2} neurons caused a potent increase in wakefulness lasting approximately 9 h and concomitantly decreased both NREM and REM sleep (Fig. 3b). CNO administration (3 mg/kg) resulted in a 139.97% increase in total wakefulness, as well as 81.63% and 94.51% reduction in NREM and REM sleep, respectively, during the 9-h post-injection period (Supplementary Fig. 1b). Compared with vehicle injection, chemogenetic activation of PVH^{vglut2} neurons significantly increased electroencephalographic (EEG) low delta power (0.25–1.00 Hz) and decreased high delta power (1.25–4.75 Hz) (Supplementary Fig. 1k). No sleep rebound followed the long-lasting wakefulness, as indicated by no change in the time spent in NREM sleep during the following dark period (19:00–07:00; Supplementary Fig. 1j). Besides, there is no significant difference in the EEG power density of NREM sleep during the day (7:00–18:00) before/after the day of CNO injection (Supplementary Fig. 1l). Similarly, CNO injection during the dark period also significantly increased wakefulness and induced high levels of arousal (Supplementary Fig. 2a, b), further demonstrating that activation of PVH^{vglut2} neurons prolonged arousal even during the dark (active) period.

Next, we further explored arousal-promoting roles of subtype neurons of PVH^{vglut2} neurons (PVH^{CRH} and PVH^{AVP} neurons) and found that chemogenetic activation of PVH^{CRH} neurons caused a potent increase in wakefulness lasting approximately 3 h and concomitantly decreased both NREM and REM sleep (Fig. 3d). CNO administration (3 mg/kg) induced a 75.7% increase in wakefulness and a 67.7%, 46% reduction in NREM and REM sleep during 3-h post-injection period (Supplementary Fig. 1e), whereas chemogenetic activation of PVH^{AVP} neurons had no effect on the amount of wakefulness ((Fig. 3f and Supplementary Fig. 1h).

Optogenetic activation of PVH ^{vglut2} neurons initiates wakefulness. Compared with the temporal precision of chemogenetic activation, optogenetic manipulations can achieve millisecond-scale control of neuronal activity. Therefore, we next employed optogenetic methods to elucidate the causal role of the PVH in controlling wakefulness. We stereotaxically injected AAVs expressing channelrhodopsin-2 (AAV-DIO-ChR2-mCherry) into the PVH (Fig. 4a). Functional expression of ChR2 was verified by *in-vitro* electrophysiology (Fig. 4b). Next, we applied optical blue-light stimulation (10 ms, 20 Hz, 20–30 mW/mm^2) after the onset of stable NREM or REM sleep during the light phase (Fig. 4c). Optical stimulation of PVH^{vglut2} neurons during NREM sleep reliably induced transitions to wakefulness in a frequency-dependent manner (Fig. 4d). Analysis of the probability of transitions between each pair of sleep-wake states showed that optical stimulation significantly enhanced the probability of wakefulness, along with a complementary decrease in the probability of NREM or REM sleep (Fig. 4e). To test whether these neurons also contributed to the maintenance of wakefulness, photostimulation was given for 1 h during the light period (09:00–10:00). Sustained activation of PVH^{vglut2} neurons via semi-chronic optical stimulation (10-ms blue-light pulses at 20 Hz for 25 s, every 60 s for 1 h) significantly increased the amount of wakefulness in ChR2-mCherry mice compared with that of the baseline control between 09:00 and 10:00 (12.3 ± 1.8 min at baseline vs. 48.6 ± 1.5 min after stimulation, n = 5; Fig. 4f). These findings demonstrate

that optogenetic activation of PVH^{vglut2} neurons potently enhanced both the initiation and maintenance of wakefulness.

PVH ^{vglut2} neurons promote wakefulness via PB and LSv connections. We next sought to determine the downstream targets by which PVH^{vglut2} neurons promote wakefulness. Specifically, AAV-hSyn-DIO-ChR2-mCherry or AAV-hSyn-DIO-mCherry constructs were injected into the PVH of Vglut2-Cre mice. We found that PVH^{vglut2} neurons mainly projected to two neuroanatomical sites: the PB (Fig. 5a) and LSv (Fig. 5e). To identify the neuronal circuits mediating the wake-promoting effect of PVH^{vglut2} neurons, ChR2 was expressed in the PVH with optic fibers targeting terminals in the PB or LSv (Fig. 5a, e). Optogenetic stimulation (10-ms pulses at 10 Hz for 2 s) of the ChR2-expressing PVH terminals evoked excitatory postsynaptic currents (EPSCs) in most of the patch-recorded PB (n = 6 cells, Fig. 5b) or LSv neurons (n = 8 cells, Fig. 5f). Moreover, 20-Hz stimulation of the bilateral PB or LSv induced a shorter transition from NREM sleep to wakefulness (latency for PB: 1.0 ± 0.8 s, latency for LSv: 1.2 ± 0.9 s) compared with that in the control (Fig. 5c, g). Analysis of the probability of transitions between each pair of sleep-wake states showed that optical stimulation significantly enhanced the probability of wakefulness, along with a complementary decrease in the probabilities of NREM and REM sleep (Fig. 5d, h). These results demonstrate that PVH→PB and PVH→LSv circuits mediated the wakefulness-controlling effect of PVH^{vglut2} neurons.

PVH ^{vglut2} neurons are necessary for the control of natural wakefulness. To determine whether PVH^{vglut2} neurons are necessary for natural wakefulness, we inhibited or ablated PVH^{vglut2} neurons with two types of AAV constructs encoding engineered Gi-coupled hM4D receptor (AAV-EF1α-DIO-hM4D(Gi)-mCherry) or caspase3 (CAGflex-taCasp3-TEVp-AAV), respectively (Fig. 6a, f). Chemogenetic inhibition of PVH^{vglut2} neurons decreased wakefulness during the 3 h following administration of CNO compared with that of vehicle (Fig. 6c). At the beginning of the dark phase (ZT15; 21:00), CNO injection induced a significant reduction in wakefulness for approximately 2 h and resulted in a 64.0% increase in NREM sleep during the 5 h post-injection period, which was accompanied by a 26.0% decrease in wakefulness (Fig. 3d). In addition, the EEG power spectrum for each state were not affected by CNO injection (Fig. 3e). Next, in order to explore the role of subtype neurons of PVH^{vglut2} neurons (PVH^{CRH}, PVH^{AVP} neurons) in controlling sleep, we inhibited these two types of neurons with AAV constructs encoding engineered Gi-coupled hM4D receptor (AAV-EF1α-DIO-hM4D(Gi)-mCherry), respectively (Supplementary Fig. 3a, e). There was no significant sleep increase found in CRH-Cre mice or AVP-Cre mice (Supplementary Fig. 3b, f), and the EEG power spectrum for each state were not affected by CNO injection (Supplementary Fig. 3d, h). These results suggested that the PVH^{vglut2} neurons might act as a critical role in regulating sleep.

To further assess the functional importance of PVH^{vglut2} neurons controlling natural wakefulness, we specifically ablated these neurons by bilaterally microinjecting AAV-EF1a-DIO-taCasp3-TEVp into the PVH region of Vglut2-Cre mice. This construct expressed a designer pro-caspase-3 (pro-taCasp3) in the PVH, the activation of which causes apoptosis (Fig. 6f, g). Compared with that of the control group, mice that underwent PVH^{vglut2} neuronal ablation showed a 28.6% decrease in the amount of wakefulness and a

74.7% increase in the amount of NREM sleep during the dark period. Similarly, ablation of PVH^{vglut2} neurons induced a 20.8% reduction in wakefulness and 30.6% increase in NREM sleep across an entire 24-h light/dark cycle (Fig. 6h). These results indicate that PVH^{vglut2} neurons are necessary for wake regulation under physiological conditions, and that dysfunction of these neurons may induce hypersomnia.

Discussion

Adequate wakefulness is essential for life and survival. In the present study, we identified the PVH as a critical hypothalamic nucleus for the regulation of wakefulness. In previous study, 15% reduction in baseline wakefulness is considered significant [6,26]. Lu *et al* have reported that lesion of the PPT and the ventral sublaterodorsal nucleus (vSLD) results in a 20–30% reduction in baseline wakefulness [6]. However, bidirectional chemogenetic manipulations that inhibit the PPT or activate SLD neurons have been shown to have little influence on baseline sleep [27,28]. In our present study, three patients with lesions mostly around the PVH showed hypersomnolence lasting above 20 h per day. PSG recordings from these patients showed that stage-two NREM was strikingly dominant, indicating that these patients slept stably and were not easily awakened. Importantly, we found that following recovery from injury around the PVH in one of these patients, the proportion of stage-two NREM sleep decreased, and this patient was concomitantly better able to stay awake. Furthermore, ablation of PVH^{vglut2} neurons in mice induced a 30.6% reduction in wakefulness across the 24-h light/dark cycle, highlighting the significance of PVH^{vglut2} neurons in maintaining wakefulness and preventing hypersomnia. Besides, in our murine experiments, no sleep rebound was seen after PVH^{vglut2}-activation-induced enhancement of wakefulness. This finding is in accordance with previous studies using chemogenetics to specifically activate wake-promoting neuronal populations [9,28–30] and indicates that chemogenetic activation of wake-promoting neuronal populations does not enhance the homeostatic drive for sleep. Taken together, our present findings provide evidence of the sufficient and necessary wake-promoting action of PVH^{vglut2} neurons in preventing hypersomnia.

The PVH is composed of abundant, diverse, and functionally distinct groups of neuroendocrine neurons, including CRH, AVP neurons [23–25,31–33]. The PVH is estimated to consist of approximately 56,000 neurons in humans [34], of which 21,000 neurons express AVP, and 2,000 neurons express CRH [35–37]. Over 90% of PVH^{CRH} neurons express vglut2 mRNA [22]. Morphological analysis has revealed that 50% of PVH^{CRH} neurons colocalize with PVH^{AVP} neurons, which regulate stress, fear, and immune responses, as well as neuroendocrine and autonomic functions [23,25,33,38,39]. There is mounting evidence that exposure to various stressors induces CRH release into the peripheral circulation [40]. Considering that PVH^{CRH} neurons are actively involved in stress-related behaviors, our results suggest that PVH^{CRH} neurons play an important role in stress-related insomnia.

The PVH has distinct input and output connections that participate in various brain functions. PVH^{vglut2} neurons are connected to the BF [41], and PVT [42], and project to the nucleus of the solitary tract (NTS) [43], lateral parabrachial nucleus (L-PBN) [16,17], pre-locus coeruleus (pLC) [31] and ventral lateral septum (LSv) [33]. Our present findings identified two specific neural circuits, among which the PVH^{vglut2}→PB/LSv circuit rather than the PVH ^{vglut2}→NTS circuit was required for the maintenance of physiological wakefulness. Glutamatergic neurons in the L-PB are necessary for arousal in response to CO_2 [18]; therefore, the PVH^{vglut2}→L-PB circuit may be involved in OSA. Xu *et al* reported that photostimulation of PVH^{vglut2}→LSv projections mediates stress-related self-grooming and fear-like jumping behaviors [33]. Thus, the PVH orchestrates sleep/wake states related to stress and chemicals through different circuits.

In conclusion, our results indicate that the PVH is a key arousal-controlling nucleus in which PVH^{vglut2}, PVH^{CRH} neurons are critical for wakefulness.

Methods

Animals. Vglut2-Cre mice were obtained from Jackson Laboratory (Bar Harbor, Maine, USA). CRH-Cre mice were obtained from the Shanghai Model Organisms Center. AVP-Cre mice were generously provided by Ying-Xu. Mice were housed in a soundproof room at an ambient temperature of 24 ± 0.5 °C, with a relative humidity of 60 ± 2%. A 12-h light/dark cycle (100 Lux, light on at 07:00) was automatically controlled[47]. Food and water were available *ad libitum*. Male heterozygous mice at 6–8 weeks of age were used for all experiments. All animal experiments were approved by the Medical Experimental Animal Administrative Committee of Shanghai. All experimental procedures involving animals were approved by the Animal Experiment and Use Committee of Fudan University (20150119–067).

Preparation of viral vectors. The AAVs of serotype rh10 for AAV-hSyn-DIO-hM3Dq-mCherry, AAV-hSyn-DIO-hM4Di-mCherry, AAV-hSyn-DIO-ChR2-mCherry, AAV-hSyn-DIO-mCherry, and AAV-CAG-FLEX-taCasp3-TEVp were used. AAV vectors were packaged into serotype 2/9 vectors, which consisted of AAV2 ITR genomes coupled with AAV9 serotype capsid proteins. The final viral concentrations of the transgenes were in the range of $1–5 \times 10^{12}$ viral particles/mL.

Surgery and injection of viral vectors. All mice were anesthetized with chloral hydrate (360 mg/kg, i.p.) for surgical procedures and were placed in a stereotaxic apparatus (RWD, Shenzhen, China). The skin above the skull was cut, a burr hole was made, and a small craniotomy was performed above the PVH. AAV constructs were slowly injected (30 nL/min) into the bilateral PVH (70 nL for each position; AP = -0.5 mm; ML = ± 0.2 mm; DV = -4.2 mm) for PSG recordings and brain-slice electrophysiology, or were unilaterally injected into the PVH for neuronal tracing. The glass pipette was left in the brain for an additional 10 min following injections and was then slowly withdrawn. All mice were implanted with electrodes for EEG and EMG recordings that were used for *in-vivo* tests at four weeks after injections under anesthesia of chloral hydrate (intraperitoneal, 360 mg/kg). The implant consisted of two stainless steel screws (1 mm in diameter), and EEG electrodes were inserted through the skull (+ 1.5 mm anteroposterior; -2.0 mm

mediolateral from bregma or lambda), while two flexible silver wires were inserted into the neck muscles. The electrodes were attached to a mini-connector and were fixed to the skull with dental cement. The scalp wound was sutured, and the mouse was when kept in a warm environment until it resumed normal activity.

Polysomnographic recordings and analysis. After a 2–3-week recovery period, each mouse was individually housed in a recording chamber and habituated to the recording cable for 2–3 days before electrophysiological recordings. Simultaneous EEG/EMG recordings were carried out with a slip ring so that movement of the mice would not be restricted. For experiments using designer receptors exclusively activated by designer drugs (DREADDs), the recordings started at 07:00 (i.e., at the beginning of the light period), and each mouse received either vehicle or CNO (3 mg/kg, C2041, LKT) treatment for two consecutive days at 09:00 (inactive period) or 21:00 (active period). As previously described[10,48], EEG/EMG signals were amplified and filtered (0.5–30 Hz for EEG, 40–200 Hz for EMG), and were then digitized at 128 Hz and recorded with SleepSign software (Kissei Comtec, Nagano, Japan). Sleep–wake states were automatically classified into 4-s epochs as follows: wakefulness was considered to have desynchronized EEG and high levels of EMG activity, NREM sleep was considered to have synchronized, high-amplitude, low-frequency (0.5–4 Hz) EEG signals in the absence of motor activity; and REM sleep was considered to have pronounced theta-like (4–9 Hz) EEG activity and muscle atonia. All scoring was automated based on EEG and EMG waveforms in 4-s epochs for both chemogenetic and optogenetic studies.

Optogenetic stimulation. Before the testing day, mice were given one day to adapt to optical fiber cables (0.8-m long, 200-μm diameter; RWD) that were placed inside the implanted fiber cannulae. On the testing day, 473-nm laser pulses (10 ms, 20 Hz) were delivered via an optic cable (Newton Inc., Hangzhou, China) using a pulse generator. Light pulse trains were generated via a stimulator (SEN-7103, Nihon Kohden, Japan) and delivered through an isolator (ss- 102J, Nihon Kohden). For acute photostimulation, each stimulation epoch was applied at 20 s after identifying a stable NREM or REM sleep event via real-time online EEG/EMG analysis. Light pulse trains (5-ms pulses of various frequencies and durations) were programmed and conducted during the inactive period. For chronic photostimulation, programmed light pulse trains (5-ms pulses at 20 Hz for 10 s and at 30-s intervals for 1 h) were used. The 473-nm laser stimulation was performed from 09:00 to 10:00. Baseline EEG/EMG recordings were acquired at the same time of day on the previous day prior to laser stimulation. Sleep–wake cycle parameters (e.g., durations of NREM sleep, REM sleep, and wakefulness, as well as sleep–wake transitions) were scored over an entire hour for each mouse. After receiving photostimulation, mice were sacrificed at 30 min after the final stimulation for subsequent c-Fos staining.

In-vitro electrophysiological recordings. At 3–4 weeks after AAV-ChR2 injections, Vglut2-Cre mice were anesthetized and transcardially perfused with ice-cold slicing buffer containing the following (in mM): 213 sucrose, 26 $NaHCO_3$, 10 glucose, 0.1 $CaCl_2$, 3 $MgSO_4$, 2.5 KCl, 1.25 NaH_2PO_4, 2 sodium pyruvate, and 0.4 ascorbic acid. The buffer was saturated with 95% O_2 and 5% CO_2. Brains were then rapidly removed, and acute coronal slices (300 μm) containing the PVH were cut using a vibratome (Leica VT 1200S,

Nussloch, Germany). Next, slices were transferred to a holding chamber containing normal recording artificial cerebrospinal fluid (aCSF) containing the following (in mM): 119 NaCl, 26 $NaHCO_3$, 25 glucose, 2.5 KCl, $2CaCl_2$, 1.25 NaH_2PO_4, and 1.0 $MgSO_4$. After being transferred, splices were allowed to recover for 30 min at 32 °C. Then, slices were maintained at room temperature for at least 30 min before recordings. During recordings, slices were transferred to and submerged in a recording chamber in which oxygenated aCSF was continuously perfused.

Expression of ChR2 was confirmed by visualization of mCherry fluorescence in PVH neuronal somata and axonal terminals. Neurons were identified and visualized with an upright microscope (Olympus, Japan) equipped with differential contrast optics, including a 40 × water-immersion objective lens (BX51WI, Olympus). Images were detected with an infrared-sensitive CCD camera (OptiMOS, Q-imaging). Patch-clamp recordings were performed with capillary glass pipettes filled with an intrapipette solution containing the following (in mM): 130 potassium gluconate, 10 KCl, 10 Hepes, 0.5 EGTA, 4 ATP-Mg, 0.5 GTP-Na, and 10 phosphocreatine, adjusting to a pH of 7.2–7.4 with KOH.

Whole-cell patch-clamp recordings were obtained using a MultiClamp 700B amplifier (Molecular Device, Union City, CA, USA) and a Digidata 1440A A/D converter (Molecular Device). Signals were sampled at 10 kHz and filtered at 2 kHz. Data were acquired and analyzed using pClamp 10.3 software (pClamp, Molecular Devices). ChR2 stimulation was evoked using 470-nm light. In voltage-clamp experiments, the holding potential was − 70 mV. When needed, 20 μM of 2,3-dihydroxy 6-nitro-7-sulfamoyl-benzoquinoxaline-2,3-dione (NBQX, 1044, Tocris Bioscience, UK), 25 μM of d-(-)-2-amino-5-phosphonopentanoic acid (D-AP5, 0106, Tocris Bioscience, UK), and 10 μM of SR95531 (SR, ab144487, Abcam Biochemicals, UK) were added to block N-methyl-D-aspartic acid receptor (NMDA), α-Amino-3-hydroxy-5-methyl-4-isoxazolepropionic acid (AMPA), and gamma aminobutyric acid A (GABAA) receptors, respectively.

Fiber photometry. Following AAV-EF1α-DIO-GCaMP6f injections, an optical fiber (125-μm outer diameter, 0.37 numerical aperture; Newdoon, Shanghai) was placed in a ceramic ferrule and was inserted toward the PVH. Fiber photometry[49] uses the same fiber to both excite and record from GCaMP in real time. After surgery, mice were individually housed for at least 10 days to recover. Fluorescent signals were acquired with a laser beam passed through a 488-nm excitation laser (OBIS 488LS; Coherent), reflected off a dichroic mirror (MD498; Thorlabs), focused by an objective lens (Olympus), and coupled through a fiber collimation package (F240FC-A, Thorlabs) into a patch cable connected to the ferrule of an upright optic fiber implanted in the mouse via a ceramic sleeve (125 μm O.D.; Newdoon, Shanghai). GCaMP6 fluorescence was bandpass filtered (MF525–39, Thorlabs) and collected by a photomultiplier tube (R3896, Hamamatsu). An amplifier (C7319, Hamamatsu) was used to convert the photomultiplier-tube current output to voltage signals, which were further filtered through a low-pass filter (40-Hz cut-off; Brownlee 440). The photometry voltage traces were down-sampled using interpolation to match the EEG/EMG sampling rate of 512 Hz via a Power1401 digitizer and Spike2 software (CED, Cambridge, UK).

Photometry data were exported to MATLAB R2018b mat files from Spike2 for further analysis. We segmented the value of the fluorescent change (ΔF/F) by calculating $(F - F_0)/F_0$, where F_0 is the baseline of the fluorescent signal. We recorded data for 3–5 h per mouse for the analysis of sleep–wake transitions to calculate the averaged calcium signal of ΔF/F during all times of vigilant states. For analyzing state transitions, we determined each sleep-wake transition and calculated ΔF/F in a ± 40-s window around that time point.

Firing rate analysis. Electrophysiological data were filtered with a band-pass filter (300–6,000 Hz) to obtain neuronal spikes. Single-unit activities were sorted according to a threshold and shape detector using principal component analysis via Offline Sorter software (Plexon Co, USA). The first two principal components of each spike on the two-dimensional plot of detected spike events were extracted. Waveforms with similar principal components were clustered via a K-means sorting method. The isolated cluster was considered as a single unit recorded from the same neuron. Spikes with inter-spike intervals < 2 ms were discarded. Cross-correlation histograms were used to eliminate cross-channel artifacts. NeuroExplorer software (version 5.0) was used for producing firing-rate rastergrams, and Prism (version 7.0) was used for producing firing-rate histograms.

Histology and immunohistochemistry. For dual immunostaining with c-Fos and mCherry, mice were deeply anesthetized with chloral hydrate (400 mg/kg) and were perfused with phosphate-buffered saline (PBS) followed by 4% PFA in 0.1-M phosphate buffer. The brain was then dissected and fixed in 4% PFA at 4 °C overnight. Fixed samples were sectioned into 30-μm coronal sections using a freezing microtome (CM1950, Leica, Germany). For immunohistochemistry, the floating sections were washed in PBS and were then incubated in the following primary antibodies in PBS containing 0.3% Triton X-100 (PBST) at 4 °C: anti-rabbit c-Fos (1:10000 for 48 h); primary antibody (Millipore); and anti-mouse NeuN (1:1000 for 12 h; MAB377, Millipore). Primary antibodies were washed five times with PBS before incubation with secondary antibodies at room temperature for 2 h (Alexa 488, 1:1000; abcam). Finally, the sections were mounted on glass slides, dried, dehydrated, and cover-slipped. Fluorescent images were collected with a confocal microscope (Nikon AIR-MP).

Statistical analysis. All data are expressed as the mean ± standard error of the mean (SEM). Sample sizes were chosen based on previous studies [48,50]. Two-way repeated-measures analysis of variance (ANOVA) was used to perform group comparisons with multiple measurements. Paired and unpaired t tests were used for single-value comparisons. One-way ANOVA was used to compare more than two groups, followed by *post-hoc* Tukey tests for multiple pairwise comparisons. Prism 7.0 (GraphPad Software, San Diego, CA, USA) was used for all statistical analyses. A two-tailed $P < 0.05$ was considered statistically significant.

Declarations

Data availability

The data supporting the findings of this study are available within the article and its Supplementary Information.

Competing Interests

The authors declare no competing interests.

Author contributions

Chang-rui Chen, Zhi-Li Huang conceived and designed the experiments. Yu-Heng Zhong and Shan Jiang performed the experiments and analyzed the data. Wei Xu performed patch-clamp electrophysiology. Lei Xiao performed multichannel electrophysiological recordings. Zan Wang collected the clinical data. Chang-Rui Chen, Yu-Heng Zhong, Shan Jiang wrote the manuscript, and all of the authors helped with the revision of the manuscript.

Acknowledgements

This study was supported in part by the National Natural Science Foundation of China (81671317, 31530035, 81420108015, 31671099, 31871072, 31571103, 81701305, 81970727 and 31900738), the National Basic Research Program of China (2015CB856401), Shanghai Pujiang Program (19PJ1401800) and ZJLab, Program for Shanghai Outstanding Academic Leaders (to Zhi-Li Huang). We are grateful to Hui Dong, Ze-Ka Chen, Ya-Nan Zhao, Peng-Fei Xu, Ming-Jie Yang, Fan Yang, and An-Shu Chen for technical assistance.

References

1 Mahowald, M. W. & Schenck, C. H. Insights from studying human sleep disorders. *Nature* **437**, 1279-1285, doi:10.1038/nature04287 (2005).

2 Saper, C. B., Chou, T. C. & Scammell, T. E. The sleep switch: hypothalamic control of sleep and wakefulness. *Trends Neurosci* **24**, 726-731, doi:10.1016/s0166-2236(00)02002-6 (2001).

3 Moruzzi, G. & Magoun, H. W. Brain stem reticular formation and activation of the EEG. *Electroencephalogr Clin Neurophysiol* **1**, 455-473 (1949).

4 Xu, M. *et al.* Basal forebrain circuit for sleep-wake control. *Nat Neurosci* **18**, 1641-1647, doi:10.1038/nn.4143 (2015).

5 Carter, M. E. *et al.* Tuning arousal with optogenetic modulation of locus coeruleus neurons. *Nat Neurosci* **13**, 1526-1533, doi:10.1038/nn.2682 (2010).

6 Lu, J., Sherman, D., Devor, M. & Saper, C. B. A putative flip-flop switch for control of REM sleep. *Nature* **441**, 589-594, doi:10.1038/nature04767 (2006).

7 Chen, L. *et al.* Basal Forebrain Cholinergic Neurons Primarily Contribute to Inhibition of Electroencephalogram Delta Activity, Rather Than Inducing Behavioral Wakefulness in Mice. *Neuropsychopharmacology* **41**, 2133-2146, doi:10.1038/npp.2016.13 (2016).

8 Fuller, P. M., Sherman, D., Pedersen, N. P., Saper, C. B. & Lu, J. Reassessment of the structural basis of the ascending arousal system. *J Comp Neurol* **519**, 933-956, doi:10.1002/cne.22559 (2011).

9 Pedersen, N. P. *et al.* Supramammillary glutamate neurons are a key node of the arousal system. *Nat Commun* **8**, 1405, doi:10.1038/s41467-017-01004-6 (2017).

10 Ren, S. *et al.* The paraventricular thalamus is a critical thalamic area for wakefulness. *Science* **362**, 429-434, doi:10.1126/science.aat2512 (2018).

11 Eban-Rothschild, A., Rothschild, G., Giardino, W. J., Jones, J. R. & de Lecea, L. VTA dopaminergic neurons regulate ethologically relevant sleep-wake behaviors. *Nat Neurosci* **19**, 1356-1366, doi:10.1038/nn.4377 (2016).

12 Chemelli, R. M. *et al.* Narcolepsy in orexin knockout mice: molecular genetics of sleep regulation. *Cell* **98**, 437-451, doi:10.1016/s0092-8674(00)81973-x (1999).

13 Sherin, J. E., Shiromani, P. J., McCarley, R. W. & Saper, C. B. Activation of ventrolateral preoptic neurons during sleep. *Science* **271**, 216-219, doi:10.1126/science.271.5246.216 (1996).

14 Gerashchenko, D., Blanco-Centurion, C., Greco, M. A. & Shiromani, P. J. Effects of lateral hypothalamic lesion with the neurotoxin hypocretin-2-saporin on sleep in Long-Evans rats. *Neuroscience* **116**, 223-235, doi:10.1016/s0306-4522(02)00575-4 (2003).

15 Adamantidis, A. R., Zhang, F., Aravanis, A. M., Deisseroth, K. & de Lecea, L. Neural substrates of awakening probed with optogenetic control of hypocretin neurons. *Nature* **450**, 420-424, doi:10.1038/nature06310 (2007).

16 Guyenet, P. G. & Bayliss, D. A. Neural Control of Breathing and CO2 Homeostasis. *Neuron* **87**, 946-961, doi:10.1016/j.neuron.2015.08.001 (2015).

17 Yokota, S., Kaur, S., VanderHorst, V. G., Saper, C. B. & Chamberlin, N. L. Respiratory-related outputs of glutamatergic, hypercapnia-responsive parabrachial neurons in mice. *J Comp Neurol* **523**, 907-920, doi:10.1002/cne.23720 (2015).

18 Kaur, S. *et al.* Glutamatergic signaling from the parabrachial nucleus plays a critical role in hypercapnic arousal. *J Neurosci* **33**, 7627-7640, doi:10.1523/jneurosci.0173-13.2013 (2013).

19 Bollu, P. C., Manjamalai, S., Thakkar, M. & Sahota, P. Hypersomnia. *Mo Med* **115**, 85-91 (2018).

20 Vong, L. *et al.* Leptin action on GABAergic neurons prevents obesity and reduces inhibitory tone to POMC neurons. *Neuron* **71**, 142-154, doi:10.1016/j.neuron.2011.05.028 (2011).

21 Xu, Y. *et al.* Glutamate mediates the function of melanocortin receptor 4 on Sim1 neurons in body weight regulation. *Cell Metab* **18**, 860-870, doi:10.1016/j.cmet.2013.11.003 (2013).

22 Ziegler, D. R., Cullinan, W. E. & Herman, J. P. Organization and regulation of paraventricular nucleus glutamate signaling systems: N-methyl-D-aspartate receptors. *J Comp Neurol* **484**, 43-56, doi:10.1002/cne.20445 (2005).

23 Zhang, X. *et al.* Brain control of humoral immune responses amenable to behavioural modulation. *Nature* **581**, 204-208, doi:10.1038/s41586-020-2235-7 (2020).

24 Sterley, T. L. *et al.* Social transmission and buffering of synaptic changes after stress. *Nat Neurosci* **21**, 393-403, doi:10.1038/s41593-017-0044-6 (2018).

25 Holmes, M. C., Antoni, F. A., Aguilera, G. & Catt, K. J. Magnocellular axons in passage through the median eminence release vasopressin. *Nature* **319**, 326-329, doi:10.1038/319326a0 (1986).

26 Lu, J., Jhou, T. C. & Saper, C. B. Identification of wake-active dopaminergic neurons in the ventral periaqueductal gray matter. *J Neurosci* **26**, 193-202, doi:10.1523/jneurosci.2244-05.2006 (2006).

27 Kroeger, D. *et al.* Cholinergic, Glutamatergic, and GABAergic Neurons of the Pedunculopontine Tegmental Nucleus Have Distinct Effects on Sleep/Wake Behavior in Mice. *J Neurosci* **37**, 1352-1366, doi:10.1523/jneurosci.1405-16.2016 (2017).

28 Erickson, E. T. M., Ferrari, L. L., Gompf, H. S. & Anaclet, C. Differential Role of Pontomedullary Glutamatergic Neuronal Populations in Sleep-Wake Control. *Front Neurosci* **13**, 755, doi:10.3389/fnins.2019.00755 (2019).

29 Anaclet, C. *et al.* Basal forebrain control of wakefulness and cortical rhythms. *Nat Commun* **6**, 8744, doi:10.1038/ncomms9744 (2015).

30 Venner, A., Anaclet, C., Broadhurst, R. Y., Saper, C. B. & Fuller, P. M. A Novel Population of Wake-Promoting GABAergic Neurons in the Ventral Lateral Hypothalamus. *Curr Biol* **26**, 2137-2143, doi:10.1016/j.cub.2016.05.078 (2016).

31 Li, M. M. *et al.* The Paraventricular Hypothalamus Regulates Satiety and Prevents Obesity via Two Genetically Distinct Circuits. *Neuron* **102**, 653-667 e656, doi:10.1016/j.neuron.2019.02.028 (2019).

32 Hung, L. W. *et al.* Gating of social reward by oxytocin in the ventral tegmental area. *Science* **357**, 1406-1411, doi:10.1126/science.aan4994 (2017).

33 Xu, Y. *et al.* Identification of a neurocircuit underlying regulation of feeding by stress-related emotional responses. *Nat Commun* **10**, 3446, doi:10.1038/s41467-019-11399-z (2019).

34 Morton, A. A quantitative analysis of the normal neuron population of the hypothalamic magnocellular nuclei in man and of their projections to the neurohypophysis. *J Comp Neurol* **136**, 143-157, doi:10.1002/cne.901360203 (1969).

35 Wierda, M. *et al.* Oxytocin cell number in the human paraventricular nucleus remains constant with aging and in Alzheimer's disease. *Neurobiol Aging* **12**, 511-516, doi:10.1016/0197-4580(91)90081-t (1991).

36 Purba, J. S., Hofman, M. A., Portegies, P., Troost, D. & Swaab, D. F. Decreased number of oxytocin neurons in the paraventricular nucleus of the human hypothalamus in AIDS. *Brain* **116 (Pt 4)**, 795-809, doi:10.1093/brain/116.4.795 (1993).

37 Purba, J. S. *et al.* Increased number of corticotropin-releasing hormone expressing neurons in the hypothalamic paraventricular nucleus of patients with multiple sclerosis. *Neuroendocrinology* **62**, 62-70, doi:10.1159/000126989 (1995).

38 Kondoh, K. *et al.* A specific area of olfactory cortex involved in stress hormone responses to predator odours. *Nature* **532**, 103-106, doi:10.1038/nature17156 (2016).

39 Mezey, E., Kiss, J. Z., Skirboll, L. R., Goldstein, M. & Axelrod, J. Increase of corticotropin-releasing factor staining in rat paraventricular nucleus neurones by depletion of hypothalamic adrenaline. *Nature* **310**, 140-141, doi:10.1038/310140a0 (1984).

40 Winter, J. & Jurek, B. The interplay between oxytocin and the CRF system: regulation of the stress response. *Cell Tissue Res* **375**, 85-91, doi:10.1007/s00441-018-2866-2 (2019).

41 Agostinelli, L. J., Geerling, J. C. & Scammell, T. E. Basal forebrain subcortical projections. *Brain Struct Funct* **224**, 1097-1117, doi:10.1007/s00429-018-01820-6 (2019).

42 Yuan, Y. *et al.* Reward Inhibits Paraventricular CRH Neurons to Relieve Stress. *Curr Biol* **29**, 1243-1251 e1244, doi:10.1016/j.cub.2019.02.048 (2019).

43 Gasparini, S., Howland, J. M., Thatcher, A. J. & Geerling, J. C. Central afferents to the nucleus of the solitary tract in rats and mice. *J Comp Neurol* **528**, 2708-2728, doi:10.1002/cne.24927 (2020).

44 Baloyannis, S. J., Mavroudis, I., Mitilineos, D., Baloyannis, I. S. & Costa, V. G. The hypothalamus in Alzheimer's disease: a Golgi and electron microscope study. *Am J Alzheimers Dis Other Demen* **30**, 478-487, doi:10.1177/1533317514556876 (2015).

45 Purba, J. S., Hofman, M. A. & Swaab, D. F. Decreased number of oxytocin-immunoreactive neurons in the paraventricular nucleus of the hypothalamus in Parkinson's disease. *Neurology* **44**, 84-89,

doi:10.1212/wnl.44.1.84 (1994).

46 Manaye, K. F. *et al.* Selective neuron loss in the paraventricular nucleus of hypothalamus in patients suffering from major depression and bipolar disorder. *J Neuropathol Exp Neurol* **64**, 224-229, doi:10.1093/jnen/64.3.224 (2005).

47 Zhang, Z., Wang, H. J., Wang, D. R., Qu, W. M. & Huang, Z. L. Red light at intensities above 10 lx alters sleep-wake behavior in mice. *Light Sci Appl* **6**, e16231, doi:10.1038/lsa.2016.231 (2017).

48 Luo, Y. J. *et al.* Nucleus accumbens controls wakefulness by a subpopulation of neurons expressing dopamine D(1) receptors. *Nat Commun* **9**, 1576, doi:10.1038/s41467-018-03889-3 (2018).

49 Li, J. *et al.* Primary Auditory Cortex is Required for Anticipatory Motor Response. *Cereb Cortex* **27**, 3254-3271, doi:10.1093/cercor/bhx079 (2017).

50 Zhang, Z. *et al.* Superior Colliculus GABAergic Neurons Are Essential for Acute Dark Induction of Wakefulness in Mice. *Curr Biol* **29**, 637-644.e633, doi:10.1016/j.cub.2018.12.031 (2019).

Figures

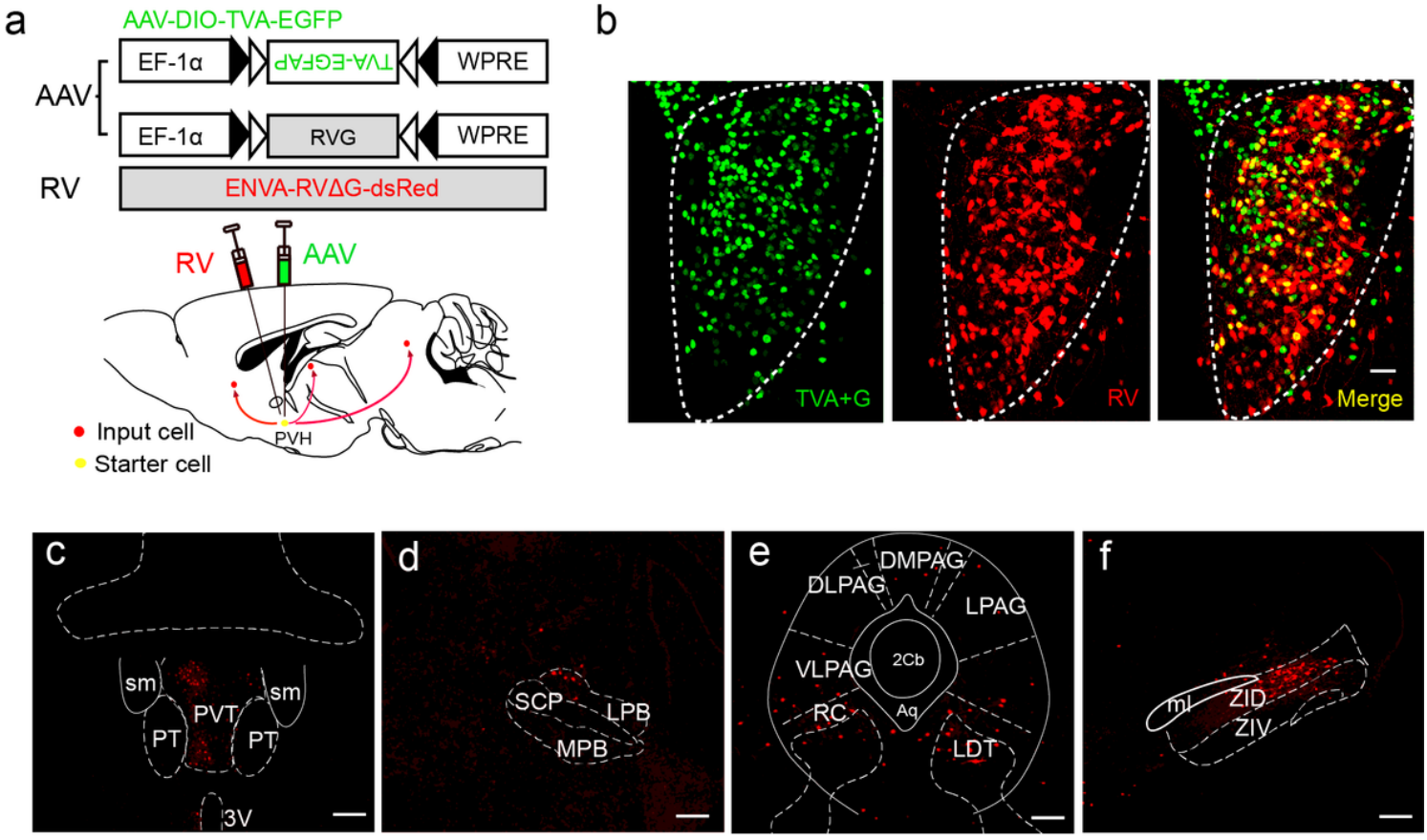

Figure 1

Whole brain presynaptic partners of PVHVglut2 neurons. a Schematic of rabies virus (RV)-mediated monosynaptic tracing. TVA, the avian tumor virus receptor A; RVΔG, glycoprotein-deleted rabies virus. b View of injection site and co-expression of TVA and RV. Green, TVA-GFP; Red, RV8 DsRed; scale bar: 50 μm. Boxed regions in b are enlarged in the right panel. Scale bars: 10 μm. c-f Representative coronal sections showing labelling of monosynaptic inputs from wake and sleep-related brain regions to PVHvglut2 neurons. Red, RV+ neurons. Scale bar: 200 μm. (c) Paraventricular thalamus (PVT); (d) parabrachial nuclei (PB); (e) Ventrolateral periaqueductal gray (VLPAG), dorsolateral periaqueductal gray (DLPAG), dorsomedial periaqueductal gray (DMPAG), laterodorsal tegmental nucleus (LDT) and raphe cap (RC); (f) Dorsal zona incerta (ZID) and ventral zona incerta (ZIV).

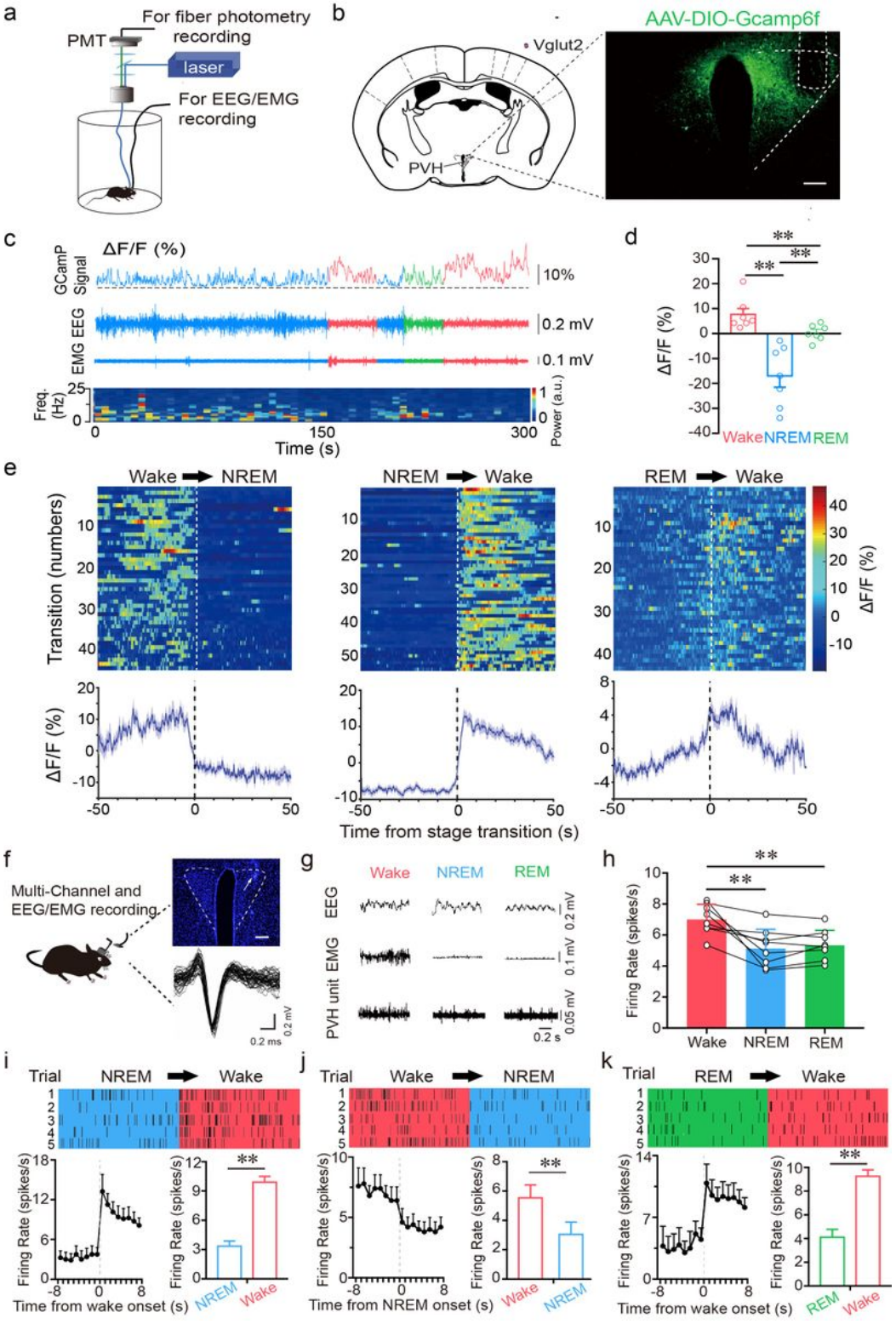

Figure 2

PVHvglut2 neurons are preferentially active during wakefulness. a Schematic of the fiber photometry setup and in-vivo recording configuration (DM dichroic mirror, PMT photomultiplier tube). b Unilateral viral targeting of AAV-EF1α-DIO-GCaMP6f into the PVH, in which the tip of the fiber optic is above the PVH. Scale bar: 200 μm. c Representative fluorescent traces, relative EEG power, and EEG/EMG traces across spontaneous sleep–wake states. ΔF/F represents the change in fluorescence from the median of the

entire time series. d Fluorescence (mean ± SEM) during wakefulness, NREM sleep, and REM sleep from three mice; the fluorescent signal was the highest during wakefulness, intermediate during REM, and the lowest during NREM sleep (n = 7 from 3 mice, one-way ANOVA followed by Tukey's post-hoc tests; $F_{6,12} = 2.94$, $P < 0.001$; P [wake vs NREM] < 0.001, P [wake vs REM] < 0.001, P [NREM vs REM] = 0.013). e Fluorescent signals aligned to sleep–wake transitions. Upper panel, Individual transitions with color-coded fluorescent intensities (NREM to wake, n = 54; wake to NREM, n = 45; REM to wake, n = 44). f Schematic configuration of in-vivo multichannel electrophysiological recordings. Upper panel: A brain slice from a mouse with electrodes implanted in the PVH. White arrow indicates the electrode track. Scale bar: 200 μm. Lower panel: Waveforms from a recorded PVH neuron. g EEG/EMG and PVH multi-unit recording traces during wakefulness, NREM sleep, and REM sleep. h Average firing rates of PVH neurons during each state (n= 8 cells from 3 mice, one-way RM ANOVA followed by LSD post hoc tests; $F_{2,14} = 12.51$, P [NREM vs wake] < 0.001, P [wake vs NREM] < 0.01, P [NREM vs REM] = 0.613). i-k Firing rates of PVH neurons during state transitions: wake-to-NREM (i), NREM-to-wake (j), and REM-to-wake transitions (k). Top: Example rastergrams of a PVH neuron during five trials of different state transitions. Bottom left: Average firing rate during the state-transition period. Bottom right: Average firing rate during 8 s before and after state transitions (P [wake–NREM] < 0.01, P [wake–NREM] < 0.01, P [REM–wake] < 0.01, paired t test). Data represent the mean ± SEM (*P < 0.05, **P < 0.01).

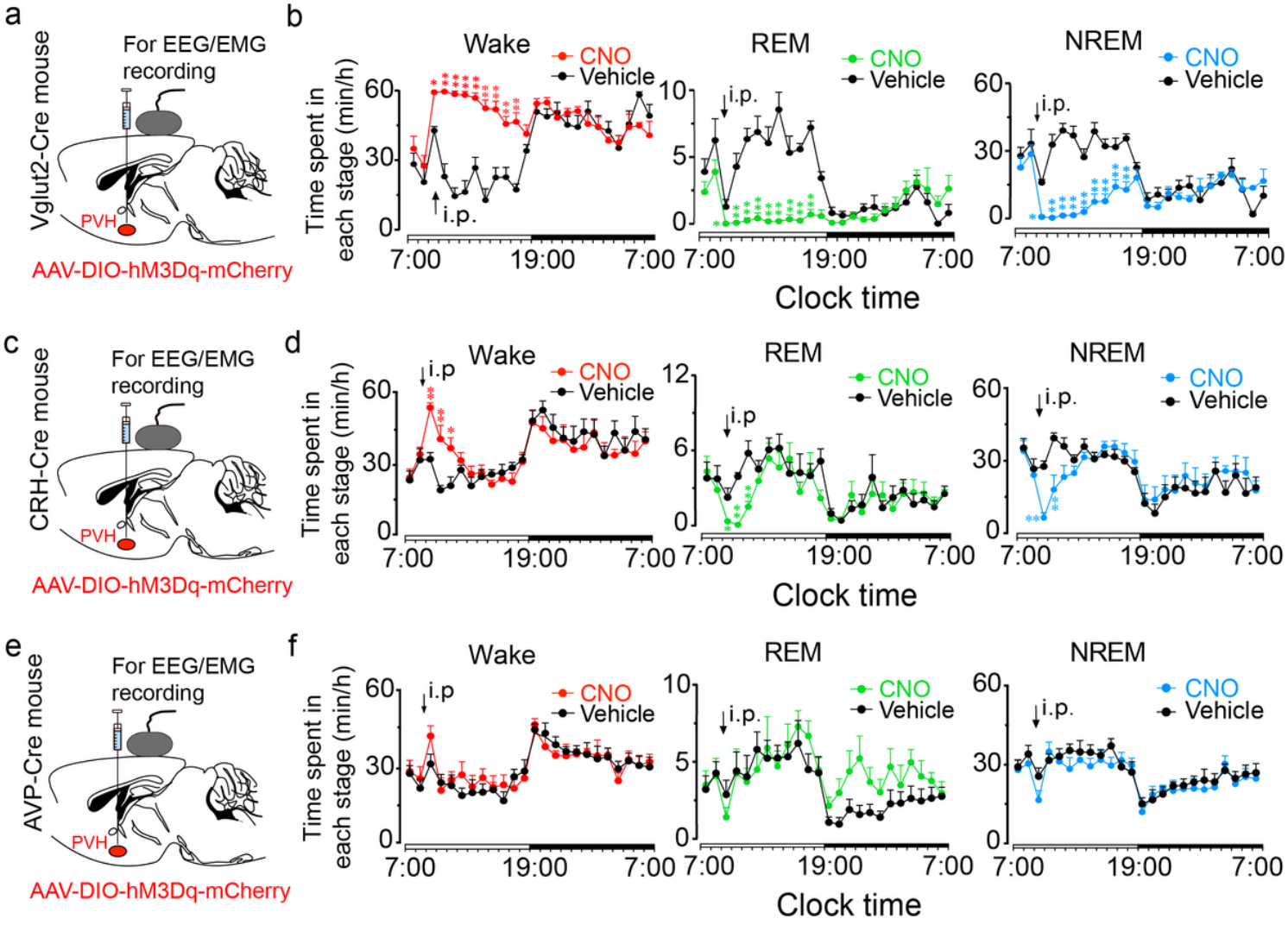

Figure 3

Chemogenetic activation of PVHvglut2, PVHCRH neurons rather than PVHAVP neurons during the light phase increases wakefulness. a, c and e Expression of AAV injection site in the PVH of Vglut2-Cre mice (a), CRH-Cre mice (c) and AVP-Cre mice (e). b, d and f Time-course changes in wakefulness, NREM sleep, and REM sleep after administration of vehicle or CNO in mice expressing hM3Dq in PVHvglut2 neurons (b, n = 7, repeated-measures ANOVA; $F_{1,12}$ = 87.09 [wake], 63.61 [NREM], 612.30 [REM]; $P < 0.001$ [wake], $P < 0.001$ [NREM], $P < 0.001$ [REM]), PVHCRH neurons (d, n = 7, repeated-measures ANOVA; $F_{1, 12}$= 0.06 [wake], 0.01 [NREM], 0.83 [REM]; $P < 0.05$ [wake], $P < 0.05$ [NREM], $P < 0.05$ [REM]) and PVHAVP neurons (f, n = 8, repeated-measures ANOVA; $F_{1, 14}$= 0.18 [wake], 1.03 [NREM], 1.94 [REM]; $P = 0.09$ [wake], 0.09 [NREM], 0.21 [REM]).

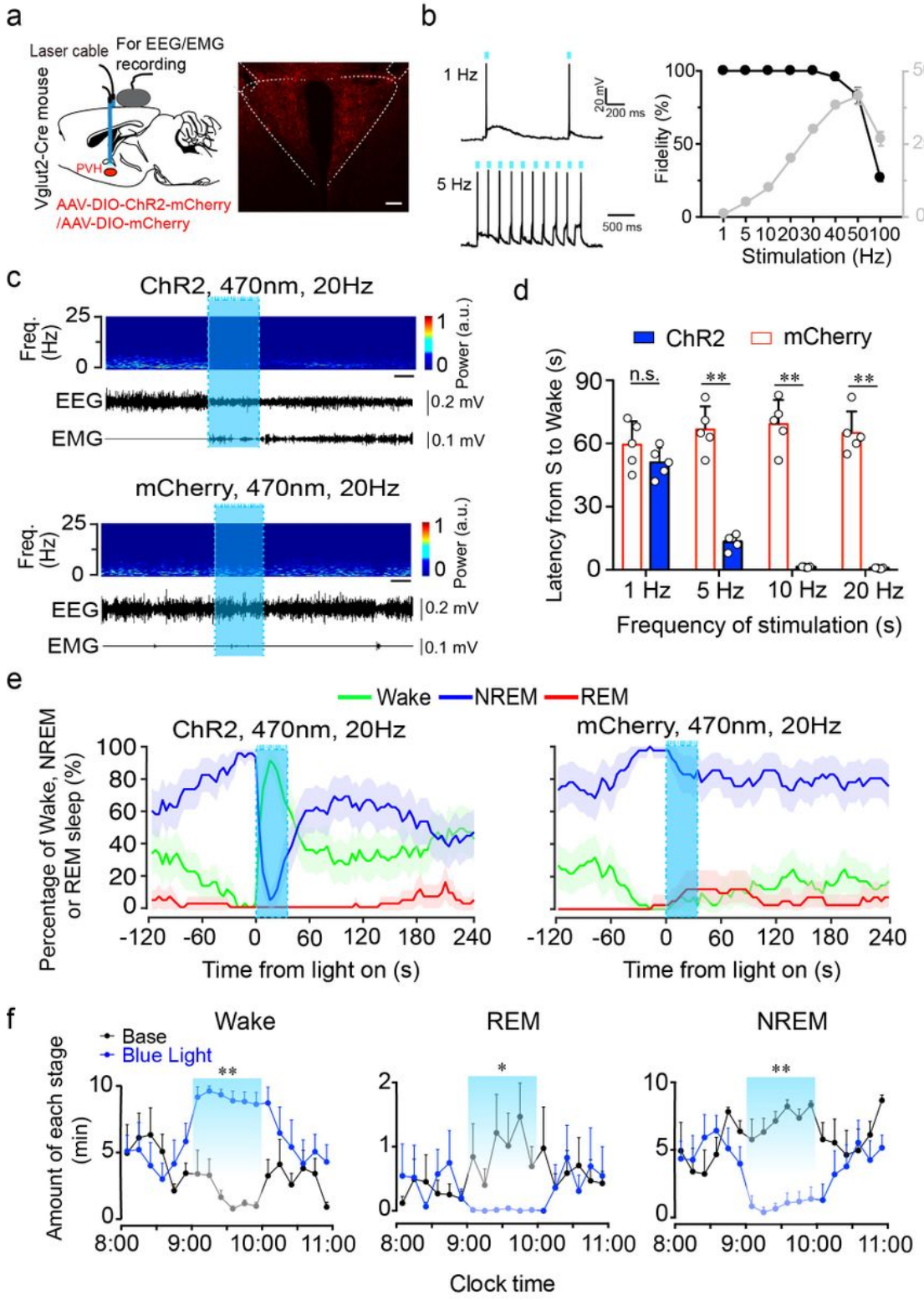

Figure 4

Optogenetic activation of PVHvglut2 neurons induces a rapid transition from NREM sleep to wakefulness. a Left: Schematic of optogenetic manipulation of PVHvglut2 neurons and EEG/EMG recordings. Right: ChR2-mCherry expression and location of optical fiber in the PVH. Scale bar: 200 μm. b Example traces (left) and fidelity of action potential firing (right) of ChR2-expressing PVH neurons evoked by 473-nm light stimulation with different frequencies. c Representative EEG/EMG traces, and heatmap

of EEG power spectra showing that acute photostimulation (20 Hz/10 ms) applied during NREM sleep induced a transition to wakefulness in a ChR2-mCherry mouse. Scale bar: 10 s. d Latencies of transitions from NREM sleep to wakefulness after photostimulation at different frequencies (n = 5, unpaired t test; 1 Hz, t8 =1.4, P = 0.19; 5 Hz, t8 = 10.29, P < 0.01; 10 Hz, t8 =13.3, P < 0.01; 20 Hz, t8 =14.04, P < 0.01). e Sleep stage after blue-light stimulation in a PVH-vglut2-ChR2 mouse or PVH-vglut2-mCherry mouse. Percentages of NREM, REM, and wakefulness during short-stimulation experiments. f Time course during semi-chronic optogenetic experiments (20 Hz/10 ms, 25-s on /35-s off). The blue column indicates the photostimulation period of the stimulation group (n = 5, repeated-measures ANOVA; F1,8 = 59.37 (wake), 18.20 (REM), 103.30 (NREM); P < 0.001 [wake], P =0.003 [REM], P <0.001 [NREM]). Data represent the mean ± SEM (*P < 0.05, **P < 0.01).

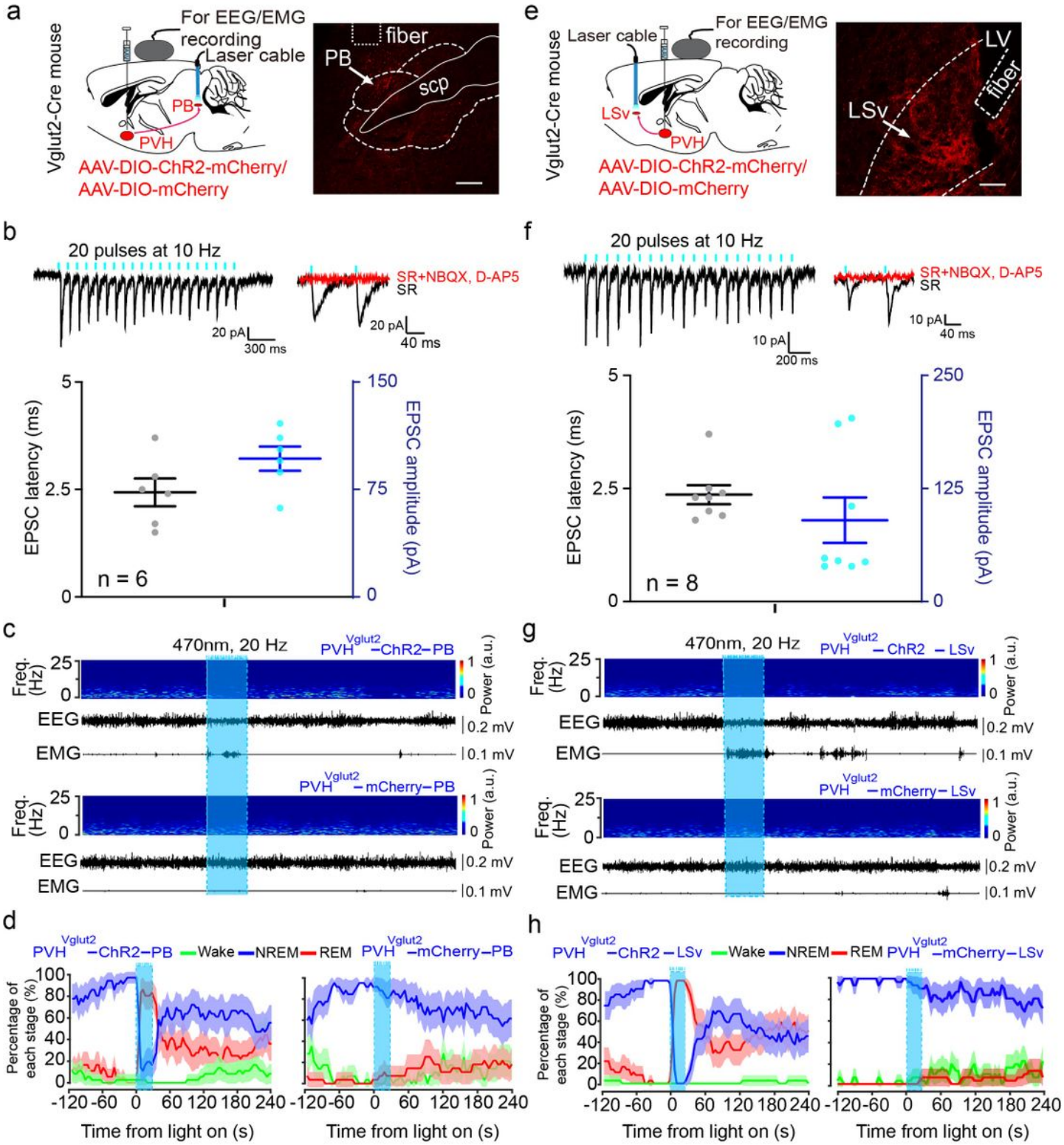

Figure 5

PVHvglut2 neurons control arousal through PB and LSv pathways. a, e Left: Schematic diagram showing the location of the optic fiber in the PB and LSv, and EEG/EMG recordings of a Vglut2-Cre mouse injected with AAV-ChR2-mCherry or AAV-mCherry in the PVH. Right: This brain section was stained against mCherry to confirm that ChR2 protein was expressed in the PVH. Scale bar: 200 μm. b, f Upper-left panel: Photostimulation-evoked EPSCs in PB neurons (b) and LSv neurons (f). Upper-right panel:

Photostimulation-evoked EPSCs were completely blocked in the presence of NBQX (20 μM) and D-AP5 (25 μM). Lower panel: Latency (left axis) and amplitude (right axis) of light-evoked EPSCs in PB neurons (b) and LSv neurons (f). c, g Representative EEG/EMG traces, and a heatmap of EEG power spectra showing that acute photostimulation (20 Hz/10 ms) applied during NREM sleep induced a transition to wakefulness in a ChR2-mCherry mouse. Scale bar: 10 s. d, h Sleep stages after PB (d) and LSv (h) blue-light stimulation in ChR2-mCherry mice or mCherry control mice.

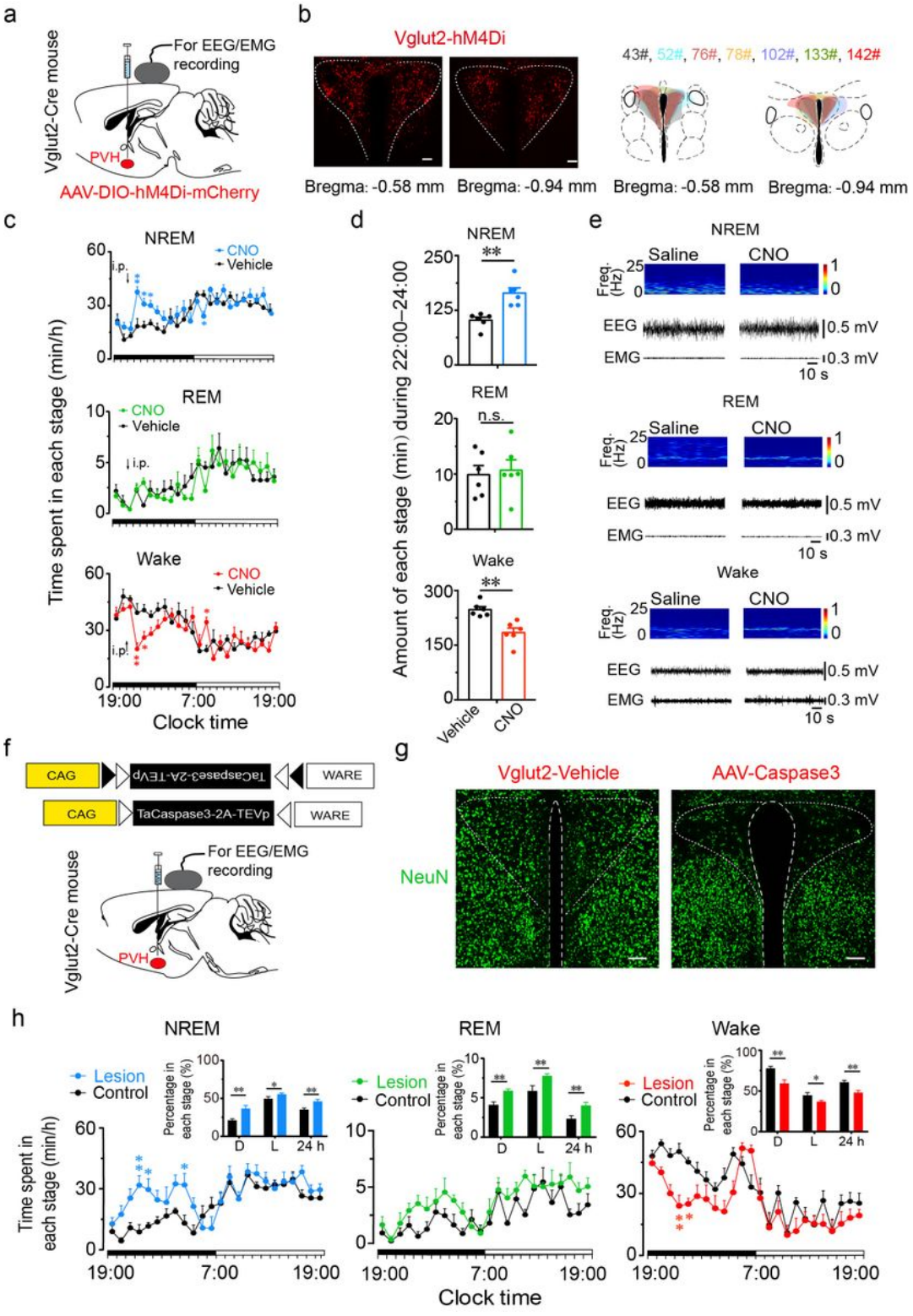

Figure 6

PVHvglut2 neurons are required for wakefulness. a Expression of AAV injection site in the PVH of Vglut2-Cre mice. b Location of hM4Di expression in the PVHvglut2 neurons. Scale bars: 200 μm. c Time-course changes in NREM sleep, wakefulness, and REM sleep after administration of vehicle or CNO in mice expressing hM4Di in PVHvglut2 neurons (n = 6, repeated-measures ANOVA; F1,10= 21.95 [wake], 7.68 [NREM], 29.23 [REM]). d Total time spent in each stage after vehicle or CNO injection (n = 6, paired t test). e Representative EEG power spectra and EEG-EMG traces of wakefulness, NREM and REM sleep after injection in Vglut2-Cre mouse. f Expression of an AAV injection site in the PVH of Vglut2-IRES-cre mice. g Image showing NeuN (neuron-specific nuclear protein) staining from a control mouse (left) and a mouse with a PVH lesion (right). Scale bars: 200 μm. h Time spent in each stage across the 24-h sleep-wake cycle. L, light phase; D, dark phase. (control group, n = 6; lesion group, n = 7, repeated-measures ANOVA; F1,10= 2.88 [wake], 2.90 [NREM], 0.06 [REM]; Inset: unpaired t test; NREM, dark phase, t11=3.27, P<0.01, light phase, t11=2.32, P=0.04, 24 h, t11=3.27, p<0.01; REM, dark phase, t11=2.94, P=0.01; light phase, t11=2.88, P=0.05; 24 h, t11=4.36, p<0.01; Wake, dark phase, t11=3.61, P<0.01; light phase, t11=2.24, P=0.05; 24 h, t11=3.56, p<0.01). Data represent the mean ± SEM (*P < 0.05, **P < 0.01).

Supplementary Files

This is a list of supplementary files associated with this preprint. Click to download.

- SupplementaryMaterials.docx